Photometric modelling of real-world objects

John Morkel and Fred Nicolls

Department of Electrical Engineering
University of Cape Town, South Africa
{jmorkel, nicolls}@dip.ee.uct.ac.za

Abstract

This paper presents a method to model the photometric properties of real-world objects from single-view and calibrated multi-view image sets. Lights are modelled as point sources and reflection properties are modelled using the isotropic Ward reflectance model. Lighting and reflectance are simultaneously recovered using known geometry. Measured reflectance data and model results are presented along with rendered scenes generated using the photometric models. The rendered images compare closely to the original images with the colours, positions of shadows and highlights accurately reproduced.

1. Introduction

In computer graphics, an image of an object is rendered by calculating how light sources interact with objects, given the shape, the position of the lights, the reflectivity of the objects and the viewpoint of the observer. Rendering, or more specifically *forward rendering*, is widely used to create special effects and animation in television shows and films and is perhaps a more familiar concept than inverse rendering. Forward rendering involves calculating the appearance of an object when geometry, reflectance properties and lighting are known.

Inverse rendering is the logical opposite of forward rendering. It is the process of decomposing a scene with unknown geometry, reflectivity and lighting into its constituent elements such that the same scene could be synthetically recreated through forward rendering. Recovering geometry, reflectance and lighting through inverse rendering when all three properties are unknown is theoretically an ill-posed problem [15], since in order to recover the lighting distribution for a scene, geometry and reflectance data for the objects in the scene are required. Similarly, to measure the reflectance data, geometry and the lighting distribution are required.

In this paper, geometry is known and is represented by a triangular mesh model consisting of vertices defined in world coordinates and a connectivity matrix. Reflectivity is represented by a *bidirectional reflectance distribution function* (BRDF) model [4, p. 61], which describes how the object's material absorbs and reflects light as the incoming light angle and viewpoint vary. The lighting distribution is modelled by an ambient light intensity and point light sources defined by a position in world coordinates and intensity.

The appearance of an object in a scene can be modelled by a geometric and a photometric model. The geometric model describes the position of the object in space and the orientations of the facets that comprise the model. The geometry of objects is assumed to be known in this paper. Geometry data is obtained using a 3D scanner. The photometric model consists of two models: a lighting model and a reflection model. The lighting model describes the light distribution of the scene in which the object is imaged and the reflection model describes how the light interacts with the surface of the object. Given these models, the object can be rendered from a novel viewpoint and under novel lighting.

This paper is organised as follows: Section 2 briefly discusses work related to this paper; Section 3 describes the process of fitting lighting and reflectance models to the data; Section 4 details the equipment, methods and calibration involved in the data acquisition process; Section 5 explains the preprocessing steps performed on the data, including aligning the 3D data with the image data, that are necessary to ensure that the different data are consistent with each other; Section 6 contains results of the reflectance and lighting measurements for the rock data. Sections 7 and 8 contain concluding remarks and possible future work.

2. Related work

A device known as a *gonioreflectometer* is traditionally used to measure the reflectance properties of an object. Recent research has led to image-based methods [11, 12, 18] that measure reflectance properties of an object without the need for specialised equipment. BRDF measurements are inherently noisy [19] and a complete estimated BRDF for an object requires many data points. BRDF models are either empirical or physics based. Model parameters are optimised so that predictions closely match BRDF measurements. BRDF models are convenient for applications in computer vision and computer graphics because an entire BRDF data set can be substituted by a few parameters. Noise is also averaged out when fitting a restricted model to the data.

Physics based models, such as the Torrance and Sparrow [17] and He-Torrance [8] models, are preferred in some literature [5, 16], but implementation is complicated because of dependence on wavelength. Low dimension models, such as the isotropic Ward model [19], are simpler to implement and provide adequate accuracy [6, 18]. Other models by Phong [14] and Lafortune et al. [9] are also widely used [1, 11, 12, 20].

3. Photometric modelling

To model the photometric properties of an object, a model of the light sources in a scene is required. This model provides

information about the intensity of the light and incidence angles for light that arrives at the object's surface. Only once a model for the scene lighting distribution is available can the reflectance properties of the object be measured.

3.1. Modelling light sources

Most reflection models describe the two fundamental types of reflection, namely diffuse and specular reflection. A simple assumption to make is that the objects in the scene exhibit only one type of reflection and not a combination, as is usually the case. The reflection is hence modelled by a single-parameter BRDF model which describes the albedo or ratio of incident to reflected light. This parameter cannot be calculated without a lighting distribution so it is assumed arbitrarily to be unity, thus the object is assumed to exhibit either perfect specular or perfect diffuse reflection.

The reflectance model used as an initial estimate should be chosen based on the typical reflectance properties of the objects to be modelled. Most objects exhibit Lambertian (or diffuse) reflection, with some exhibiting both diffuse and specular reflection. The exception is highly reflective surfaces such as mirrors, which are mainly specularly reflective. As such, the Lambertian assumption is used to infer an initial estimate for the lighting distribution.

For an object with Lambertian reflection, the intensity of a point p for a given light distribution is given by

$$I(p) = L_0 + \sum_{i=1}^{n} \mathbf{N}_p \cdot (\mathbf{V}_i - \mathbf{P}_p)\Gamma(p,i)\frac{1}{||\mathbf{V}_i - \mathbf{P}_p||^2}L_i, \quad (1)$$

where L_0 is the ambient light term that accounts for ambient light and inter-reflections, n is the number of point light sources, $\Gamma(p,i)$ is a function that is 1 when point p is visible to light source i and 0 otherwise, $\mathbf{N}_p$ is the normal vector at point p, $\mathbf{V}_i$ is the position vector for light source i, $\mathbf{P}_p$ is the position vector for the point p, and L_i is the intensity for light source i.

The vector from the point p on the surface to the light source i is $\mathbf{V}_i - \mathbf{P}_p$. The $\frac{1}{||\mathbf{V}_i - \mathbf{P}_p||^2}$ factor is the falloff in intensity that occurs as a result of the light energy being distributed over an increasingly larger area as distance from the light source increases. The falloff is inversely proportional to the square of the distance from the light source.

Light sources are modelled as points with a position in 3D space and an intensity for each of the RGB channels. There is an additional ambient light term that accounts for any background lighting that is present in the room, as well as any inter-reflection that might occur. The number of light sources is a user-defined input. Face orientation is extracted from the geometric model of the object. Selecting the correct number of light sources for the model is not critical because light sources will converge to the same point in space if there are more light sources in the model than in reality.

The position and intensity for each light source is optimised using the MATLAB non-linear optimisation routine *lsqnonlin*. The cost function employed is defined as the squared error between the intensity obtained using the rendering equation (Equation 1) and the observed intensity from image data. The point light sources are initially optimised without an ambient light term. Once good estimates for the point light sources are available, their positions and intensities are optimised in a second step along with the ambient light intensity. This lighting distribution is used as an initial estimate and is further refined when reflectance and lighting parameters are simultaneously estimated.

3.2. Modelling reflectance

The isotropic Ward model [19], used for modelling reflectivity in this research, is defined as

$$\beta(\theta_i, \phi_i, \theta_o, \phi_o) = \frac{\rho_d}{\pi} + \frac{\rho_s \exp\left(-\tan^2(\delta)/\alpha^2\right)}{4\pi\alpha^2}, \quad (2)$$

where ρ_d is the diffuse reflectance, ρ_s is the specular reflectance, α is the standard deviation of the surface slope, and δ is the angle between the half vector, $\hat{h}$, and the surface normal, $\hat{n}$. It offers a good compromise between complexity and accuracy. The Ward model does not explicitly depend on wavelength, but diffuse and specular reflectivity parameters can be calculated for each RGB channel so that colour can be modelled.

Calculating the ρ_d, ρ_s and α parameters is done by regression in an optimisation framework using the MATLAB *lsqnonlin* nonlinear optimiser. Each pixel in every image of an object provides a data point that is used to calculate optimal BRDF model parameters to fit the the observed BRDF data. Angle information is deduced from the mesh model of the object, the camera positions, and the light source positions. The viewing ray is obtained by backprojecting each pixel onto the 3D model of the object. The cost used in optimising is the squared error between the intensity of each observed pixel and the intensity calculated from the rendering equation

$$I(p) = \frac{\rho_d}{\pi}L_0 + \sum_{i=1}^{n} \beta(\theta_i, \phi_i, \theta_o, \phi_o)\Gamma(p,i)\cos(\theta_i)\frac{1}{||\mathbf{V}_i - \mathbf{P}_p||^2}L_i, \quad (3)$$

where ρ_d is the diffuse reflectance parameter of the Ward model, L_0 is the intensity of the ambient light, n is the number of light sources, $\beta(\theta_i, \phi_i, \theta_o, \phi_o)$ is the Ward BRDF model, $\Gamma(\cdot)$ is a function that is 1 when point p is visible to light source i and 0 otherwise, $\mathbf{V}_i$ is the position vector for light source i, $\mathbf{P}_p$ is the position vector for the point p, and L_i is the intensity for light source i.

Once a BRDF model for an object has been calculated, the lighting distribution can be refined using the BRDF model. Vogiatzis et al. [18] choose to alternately optimise the lighting distribution and the BRDF model until both converge. In this paper however, the BRDF model parameters and lighting distribution are optimised simultaneously, which leads to faster convergence and has a lower likelihood of converging on a local minimum.

4. Data acquisition

Four data sets are used to generate the results in this paper: two single-view data sets of marbles and two multi-view data sets of rocks. The geometry for the marbles is approximated by a sphere and therefore data does not need to be captured in these cases. Geometry data is captured for the two rock data sets.

Image data is needed for all four data sets to make reflectance measurements. A single distant point light source is used.

4.1. Capturing geometry data

The geometry of an object is represented by a 3D model that closely approximates its structure. A 3D mesh model of an object consists of vertices connected together in a mesh, with each facet of the model forming a triangle. A mesh model not only yields shape information but also contains the normal vectors for each facet. This is important for measuring the angles at which the light hits the object surface relative to the viewing angle. Measuring these two angles is fundamental in the measurement of the reflectance of an object.

Geometry data is captured using the *NextEngine Desktop 3D Scanner*. It is a multi-stripe laser triangulation 3D scanner that interfaces with its own proprietary software to produce 3D models of real world objects. The 3D models it produces are accurate up to 0.125 mm in *macro* mode and 0.375 mm in *wide angle* mode [13]. The high level of accuracy of the model means it can be used as a ground truth or baseline description of the geometry of the object.

The scanner captures colour information for each view of the object and then texture maps these images onto the 3D model. Regions of overlapping colour data are blended. The colour information captured is adequate for visualisation purposes, but qualitative experiments have shown that the colour data can contain significant errors and are not suitable for photometric modelling.

It is important to have control over the lighting conditions of the room for reflectance and lighting recovery so that ambient light and the positions and types of light sources used are well suited to capturing data for photometric modelling.

4.2. Capturing image data

Colour data is captured using a digital camera because the data acquired by the 3D scanner is not suitable for photometric modelling. A 1024×768 colour *Point Grey Flea* camera mounted on a tripod is used to capture frontlit and backlit images of the objects. The camera's gamma and gain parameters are fixed at unity so that the intensity response of the camera is as close to linear as possible and noise is minimal. The camera aperture is chosen to be just large enough so that the brightest regions of the image are almost saturated when the shutter speed is at a maximum, but small enough to maintain a large depth of field. A large depth of field ensures that all parts of the sample are in focus.

The object is positioned on top of a fluorescent lightbox to simplify silhouette extraction from the backlit images. A programmable and accurate turntable is used to change the position of the object and light source relative to the camera. The halogen light source mounted on a stand is positioned on the turntable approximately 50 cm above the object. To minimise ambient light, the room is darkened so that the halogen light source is dominant.

The turntable is used to position the object at 20 different orientations, making up a complete 360° revolution. Each orientation is rotated 18° from the previous one. The frontlit image is captured with the halogen light source on and the fluorescent lightbox off. The backlit image is captured with the opposite configuration. A frontlit and backlit image is captured for each orientation.

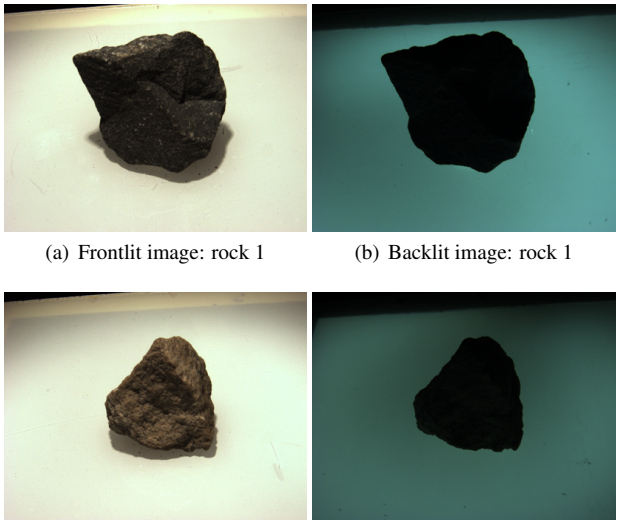

(a) Frontlit image: rock 1 (b) Backlit image: rock 1

(c) Frontlit image: rock 2 (d) Backlit image: rock 2

Figure 1: Frontlit and backlit images of objects. The frontlit image is used to extract colour information and the backlit image is used to extract the silhouette of the object.

4.3. Calibration

The images in the rock data sets are captured as a turntable sequence. A set of calibration images is captured of a checkerboard pattern positioned on the turntable, which is used to calculate the extrinsic camera parameters for each turntable position. This calibration step is performed by means of the *Camera Calibration Toolbox* for MATLAB [2].

The grid points extracted from the the turntable image sequence of the checkerboard calibration pattern are coplanar because the calibration pattern is rotating about a fixed axis. Calibrating intrinsic camera parameters requires non-coplanar grid points. As a result, the intrinsic camera parameters cannot be determined from these images. A separate set of calibration images is required with non-coplanar data points spread over the entirety of the image plane at varying depths. Intrinsic parameters, including focal length, distortion and principal point, can be determined from this calibration image sequence.

The Camera Calibration Toolbox gives a good estimate of the intrinsic and extrinsic camera parameters. However, there is a chance that the calibration results contain small errors due to slight variations in the position of the object. These variations can be brought on by vibrations from the turntable or small errors in turntable position.

A final calibration step similar to a *bundle adjustment* [7] optimises the camera parameters to minimise these errors. The silhouettes extracted from the backlit images are used to calculate the *epipolar tangency* (ET) error. ET error is defined as the

squared perpendicular distance between the tangent point on the silhouette for a particular epipole and the epipolar line. A bundle adjustment involves optimising the camera parameters for all cameras such that the ET error is a minimum. This optimisation is performed using the Levenberg-Marquardt non-linear minimisation method as implemented in the MATLAB *lsqnonlin* function.

5. Data pre-processing

Before reflectance and lighting estimates can be made from input 3D and image data, the raw data resulting from the data capture stage need to be processed to account for limitations and inaccuracies in the data capture process. The pre-processing steps include undistorting image data to remove radial and tangential distortion introduced by the camera lens, and aligning image and 3D data so that the two forms of data can be processed within the same reference frame.

5.1. Undistorting image data

When calibrating the intrinsic properties of the cameras, a 5-parameter combined radial and tangential distortion model of the camera lens is calculated. The distortion model produced by the Camera Calibration Toolbox is non-linear and hence cannot be modelled by the camera matrix. As a result, the image data are undistorted directly by generating new images with the distortion removed. Both frontlit and backlit images are undistorted. To reduce the noise in the undistorted silhouette, the silhouette is first extracted from the unprocessed image and then the extracted silhouette coordinates are undistorted. The undistortion is performed using functions from the Camera Calibration Toolbox.

5.2. Aligning image and 3D data

For measuring reflectance and lighting data from images, the colour data at points in the images must correspond to the correct points on the surface of the 3D model. This means that the coordinate system in which the cameras are specified must be aligned to the coordinate system in which the 3D model is specified. This can be achieved by transforming the vertices of the 3D model with a transformation matrix $\mathbf{T} = [\lambda\mathbf{R}\ \ \mathbf{t}]$ where λ is a scaling factor, $\mathbf{R}$ is the rotation matrix that aligns the orthogonal vectors, and $\mathbf{t}$ is the translation vector between the origins.

The transformation matrix $\mathbf{T}$ is optimised iteratively by minimising the ET error between pairs of silhouettes generated from the transformed 3D model and backlit image data. The visual hull [10], or volume of intersection of the silhouettes from each camera, is used as an approximate 3D model that lies in the same coordinate system as the cameras. A good initialisation is required for the transformation matrix to ensure convergence, especially due to the rotational degrees of freedom of the matrix.

The eigenvectors of the vertices of the 3D data form reliable orthogonal bases that have approximately the same orientation as the vertex data for both sets of 3D data. The eigenvectors are used along with the centroids of vertices of the visual hull and ground truth. The ground truth data is translated so that the origin coincides with the centroid of the vertices. The vertices are rotated so that the eigenvectors of the ground truth data are aligned with the eigenvectors of the visual hull. The vertices of the ground truth data are then translated so that the centroid coincides with that of the visual hull. The scaling factor is initialised to be the average ratio of the caliper diameter measurements [3, p. 12] along the directions defined by the orthogonal bases of the visual hull and ground truth data.

The cost function that is minimised to find the optimum transformation matrix is defined as

$$e(\mathcal{C}, \mathcal{S}, \mathbf{T}, \mathbf{V}) = \sum_{i=1}^{N-1} \sum_{j=i+1}^{N} \left[\Delta(\mathbf{C}_i, \mathbf{C}_j, \mathbf{S}_j, \beta(\mathbf{TV}, \mathbf{C}_i))\right]^2 \quad (4)$$

where $e(\cdot)$ is a function that returns the sum of squared distances between the epipolar lines and tangent points for all camera pairs, $\mathcal{C}$ is the set of cameras, $\mathcal{S}$ is the set of silhouette boundary coordinates, N is the number of views, $\mathbf{T}$ is the transformation matrix that is applied to mesh vertices $\mathbf{V}$, $\Delta(\cdot)$ is a function that returns the epipolar tangency error for a pair of cameras $\mathbf{C}_i$ and $\mathbf{C}_j$ with boundary points $\beta(\mathbf{TV}, \mathbf{C}_i)$ and $\mathbf{S}_j$, and $\beta(\cdot)$ is a function that returns the projection of vertices $\mathbf{V}$ into camera $\mathbf{C}_i$.

Figure 2 shows the initial starting point and also the result of the optimisation process of aligning the 3D model to the image data. The starting point obtained using the initial guess for the transformation matrix is close to the optimum solution. After the final iteration, the tangent points on the 3D model and epipolar lines approximately coincide, as is the expected outcome when minimising Equation 4.

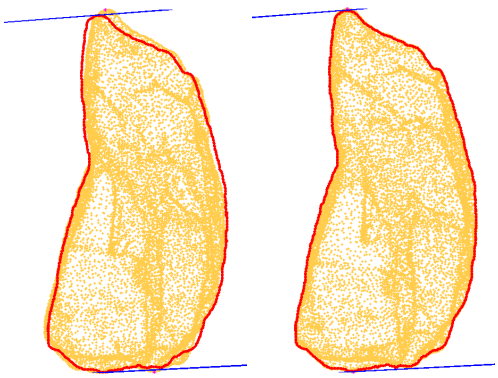

(a) Before optimisation (b) After optimisation

Figure 2: Results of aligning 3D data to image data as seen from a single viewpoint. Figures 2(a) and 2(b) show the alignment of the image silhouette (bold red outline) with the 3D model (orange points) before and after of the optimisation process respectively. The initial estimate for alignment can be seen to be a good starting point, since the silhouette and 3D model are only slightly misaligned. The image silhouette and 3D model are well aligned after the final iteration. The epipolar tangent lines can be seen in blue at the top and bottom of both images. The tangent points on the 3D model are shown in magenta and can also be seen at the top and bottom of each image.

6. Results

A representation of the positions of the point light sources is shown in Figure 3 for the rock data sets. Each image shows the objects as viewed from the positions of the point light sources in each scene, this indicates the portion of the surface that is illuminated by each light.

Figure 4 shows a spherical plot of the measured reflectance data and the model that fits the data. The data come from the first marble data set. The diffuse reflection (constant radius) and the specular highlight (radial spike) can be seen in the plot.

Figure 5 shows the results of the lighting and reflectance recovery process for four data sets comprising of two single-view data sets of an opaque glass marble and two multi-view data sets of different rocks. Figures 5(a), 5(d), 5(g) and 5(j) show the original image data with background information removed. Figures 5(b), 5(e), 5(h) and 5(k) show a rendered image of each object that is generated using only the recovered lighting distribution and reflectance parameters for each data set. The positions of the highlights and shadows in the rendered images correspond to those in the original images. Figures 5(c), 5(f), 5(i) and 5(l) are difference images that show the difference in intensity of the green colour band between the original image and the rendered image. The red and blue colour bands exhibit similar behaviour. The green colour band is used because there are twice the number of green pixels in the Bayer pattern of the colour image than red or blue. Fewer interpolation operations are required on the green data making it more accurate.

The rendered objects can be seen to closely resemble the original images. The rendered image of the first rock data set (Figure 5(h)) does not capture the spatial variation of the material present in the original image (Figure5(g)) due to the limitation that the material is assumed to be homogeneous, i.e. the appearance is modelled by one set of reflectance parameters. As a result, the reflectance parameters model the average appearance of the objects, which is especially obvious in the grey appearance of the rendered image of the first rock data set.

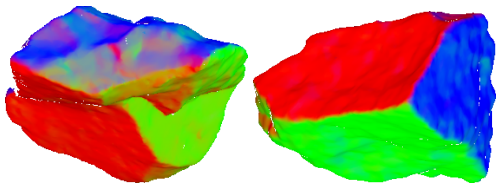

(a) Rock 1 (b) Rock 2

Figure 3: Each of the rock data sets as seen from each light source. Each view is from the position of the recovered light source and indicates which faces are lit by each light source. The colour represents an RGB encoding of the surface normals. In these scenes, lighting is represented by a single point light source and an ambient light source. Ray casting is used to determine which light sources illuminate each face.

7. Conclusion

This paper details the data capture process for measuring the reflectance properties of objects from images and highlights con-

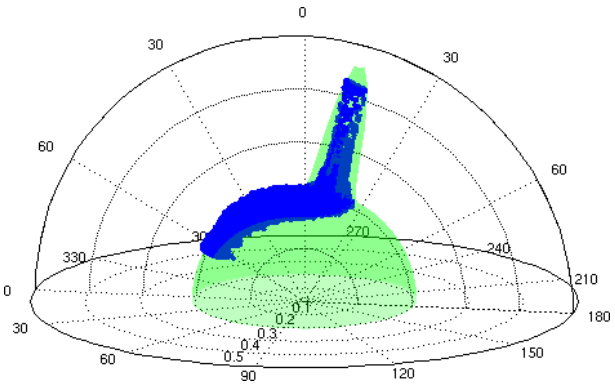

Figure 4: BRDF data and model plotted against the azimuthal and zenith angles of observation. The BRDF data are plotted as blue points with the Ward model predication plotted as a green surface. The radial spike corresponds to a specular highlight and the regions of constant radius correspond to the diffuse colour. The parameters of the Ward model shown here are $\rho_d = 0.647$, $\rho_s = 0.0127$ and $\alpha = 0.0629$.

siderations that need to be taken into account. The geometry information is captured using a NextEngine Desktop 3D Scanner, which provides more accurate data than image-based methods. Colour information is captured separately from turntable sequences and aligned with the geometry information using the epipolar tangency constraint. Ward reflectance model parameters are estimated through a regression process that matches the predicted appearance with the original image data.

Qualitative results show promise, with renderings comparing closely to original images. These results indicate that the reflectance and lighting modelling succeeds in modelling the appearance of the objects, with discrepancies only appearing when more than one material is present in an image. This and other limitations are to be addressed in future work.

8. Future work

The following avenues are envisioned as future work: a quantitative analysis of the accuracy of surface normals obtained from the visual hull as compared to 3D scanner data; an analysis of the effect on accuracy of reducing the number of triangles in the geometry model to find a balance between processing speed and accuracy; an analysis of the effect on accuracy of reducing the number of data points in the sample for reflectance and lighting recovery to find a balance between processing speed and accuracy; extending the reflectance model to account for objects made of more than one material and spatial variation in material on the surface of the object in a similar manner to Lensch et al. [11]; and colour calibration to ensure linearity in colour measurements;

9. Acknowledgements

The authors would like to thank De Beers and the National Research Foundation for their financial assistance.

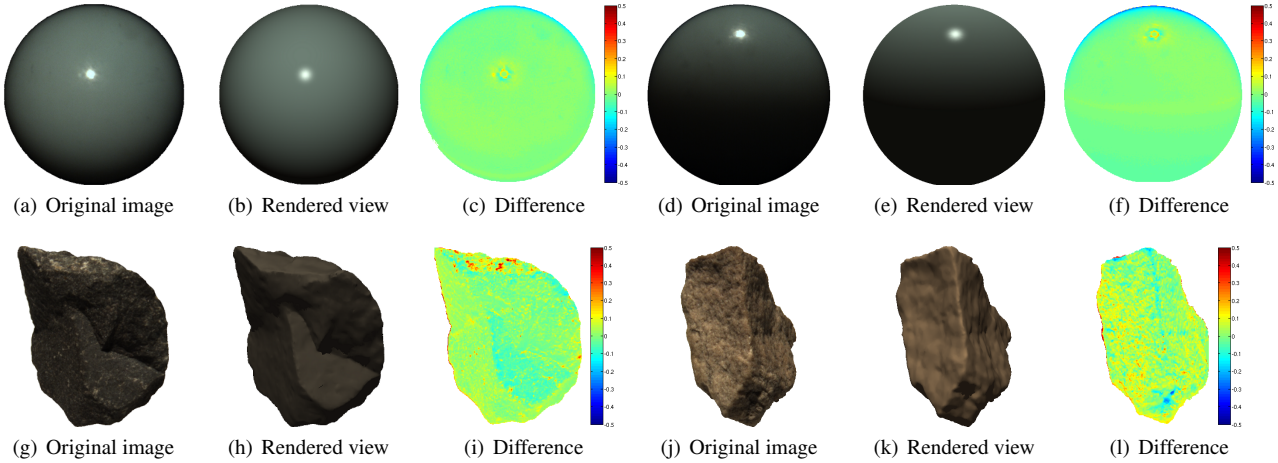

(a) Original image (b) Rendered view (c) Difference (d) Original image (e) Rendered view (f) Difference

(g) Original image (h) Rendered view (i) Difference (j) Original image (k) Rendered view (l) Difference

Figure 5: Results of lighting and reflectance recovery. Ground truth images, rendered views and difference images for the two marble data sets and the two rock data sets. The shadows and highlights in the rendered images can be seen to correspond with those in the original images. The difference images show the difference in intensity of the green colour band between the original image and the rendered image. Positive values occur when the original image is greater in intensity than the rendered image and vice versa for negative values.

10. References

[1] N. Birkbeck, D. Cobzas, P. Sturm, and M. Jägersand. Variational shape and reflectance estimation under changing light and viewpoints. In *ECCV '06, Graz, Austria*, volume 1, pages 536–549. Springer, May 2006.

[2] J.-Y. Bouguet. Camera calibration toolbox for MATLAB. URL `http://www.vision.caltech.edu/bouguetj/calibdoc/`. Last accessed 14/08/08.

[3] K. Forbes. *Calibration, Recognition, and Shape from Silhouettes of Stones*. PhD thesis, University of Cape Town, June 2007.

[4] D. A. Forsyth and J. Ponce. *Computer Vision: A Modern Approach*. Prentice Hall, 2003. ISBN 0130851981.

[5] A. S. Georghiades. Incorporating the Torrance and Sparrow model of reflectance in uncalibrated photometric stereo. In *ICCV '03*, page 816, Washington, DC, USA, 2003. IEEE Computer Society.

[6] D. B. Goldman, B. Curless, A. Hertzmann, and S. M. Seitz. Shape and spatially-varying BRDFs from photometric stereo. In *ICCV '05*, pages 341–348, Washington, DC, USA, 2005. IEEE Computer Society.

[7] R. Hartley and A. Zisserman. *Multiple view geometry in computer vision*. Cambridge University Press, 2003.

[8] X. D. He, K. E. Torrance, F. X. Sillion, and D. P. Greenberg. A comprehensive physical model for light reflection. In *SIGGRAPH '91*, pages 175–186, New York, NY, USA, 1991. ACM Press.

[9] E. P. F. Lafortune, S.-C. Foo, K. E. Torrance, and D. P. Greenberg. Non-linear approximation of reflectance functions. In *SIGGRAPH '97*, pages 117–126, New York, NY, USA, 1997. ACM Press/Addison-Wesley Publishing Co.

[10] A. Laurentini. The visual hull concept for silhouette-based image understanding. *PAMI*, 16(2):150–162, 1994.

[11] H. P. A. Lensch, J. Kautz, M. Goesele, W. Heidrich, and H.-P. Seidel. Image-based reconstruction of spatial appearance and geometric detail. *ACM Trans. Graph.*, 22 (2):234–257, 2003.

[12] S. R. Marschner, S. H. Westin, E. P. F. Lafortune, K. E. Torrance, and D. P. Greenberg. Image-based BRDF measurement including human skin. In *Eurographics Workshop on Rendering*, Granada, Spain, June 1999.

[13] NextEngine. NextEngine FAQ. URL `http://www.nextengine.com/`. Last accessed 14/08/08.

[14] B. T. Phong. Illumination for computer generated pictures. *Commun. ACM*, 18(6):311–317, 1975.

[15] R. Ramamoorthi and P. Hanrahan. A signal-processing framework for inverse rendering. In *SIGGRAPH '01*, pages 117–128, New York, NY, USA, 2001. ACM Press.

[16] Y. Sato, M. D. Wheeler, and K. Ikeuchi. Object shape and reflectance modeling from observation. In *SIGGRAPH '97*, pages 379–387, New York, NY, USA, 1997. ACM Press.

[17] K. E. Torrance and E. M. Sparrow. Theory for off-specular reflection from roughened surfaces. *Journal of Optical Society of America*, 57(9):1105–1114, 1967.

[18] G. Vogiatzis, P. Favaro, and R. Cipolla. Using frontier points to recover shape, reflectance and illumunation. In *ICCV '05*, pages 228–235, Washington, DC, USA, 2005. IEEE Computer Society.

[19] G. J. Ward. Measuring and modeling anisotropic reflection. In *SIGGRAPH '92*, pages 265–272, New York, NY, USA, 1992. ACM Press.

[20] T. Yu, N. Xu, and N. Ahuja. Recovering shape and reflectance model of non-lambertian objects from multiple views. In *CVPR '04*, volume 2, pages 226–233, Los Alamitos, CA, USA, 2004. IEEE Computer Society.